Renewable and Sustainable Energy Reviews 37 (2014) 852–866

Contents lists available at ScienceDirect

Renewable and Sustainable Energy Reviews

journal homepage: www.elsevier.com/locate/rser

Dynamic performance assessment of DFIG-based wind turbines: A review

Mohsen Rahimi *

Department of Electrical and Computer Engineering, University of Kashan, P. O. Box 87317–51167, Kashan, Iran

ARTICLE INFO

Article history:
Received 13 November 2013
Received in revised form
7 May 2014
Accepted 20 May 2014
Available online 11 June 2014

Keywords:
Doubly fed induction generator
Wind turbine
Dynamic behavior
Stator dynamics
Rotor and grid-filter
Back-Emf voltages

ABSTRACT

This paper studies the dynamic behavior of doubly fed induction generators (DFIGs) modeled with the stator flux orientation regarding rotor- and grid-side converter control strategies. The investigations include modal and sensitivity analysis, and using them to identify and characterize the instability mode, stator dynamics analysis, and time domain simulations. The paper first deals with the modal analysis of the DFIG for different control strategies and operating conditions. Then the dynamic and transient performance of the DFIG under voltage dips and large disturbances are investigated, and the effects of rotor and grid-filter control strategies on the DFIG transient behavior are examined. Increasing the rotor and grid-filter closed loop bandwidths, rotor current active damping, and compensation of back-emf voltages can improve the rotor and grid-filter dynamics, decrease tracking error and limit the rotor current transients. However they can lead to poorly stator modes and deteriorate the DFIG transient performance. Thus, appropriate selection of rotor controller parameters has an important effect on the DFIG transient performance, and consequently on the future interconnected power system.

Contents

* Tel.: +98361 5912496; fax: +98361 5912424.
E-mail address: mrahimi@kashanu.ac.ir

http://dx.doi.org/10.1016/j.rser.2014.05.072
1364-0321/

1. Introduction

There are several types of adjustable speed generators used in wind turbines [1]. The DFIG is a commonly used variable speed generator in wind turbine applications. In Fig. 1, the DFIG-based wind turbine is connected to the infinite bus through the equivalent grid impedance. It consists of a wound rotor induction generator with back-to-back voltage source converters linking the rotor to the grid. The rotor-side converter is connected to rotor windings and is used to control the generator speed and reactive power, while the grid-side converter is connected to the grid through a grid-side filter and is used to control dc bus voltage and reactive power.

Field oriented control (FOC) is the most widely used controlling method of DFIG, which enables decoupled control of real and reactive power. The FOC may be implemented as stator-flux orientation control [2], or air-gap flux orientation [3].

In recent years, DFIG-based wind turbines have been an integrated part of distributed generation system. Therefore, they will have strong effects on the future interconnected power system. In other words, any abnormality associated with the DFIG affects the power grid performance. Taking this into account, with increased penetration of wind power, the behavior of DFIG-based wind turbines under disturbances becomes more important.

This work deals with the dynamic behavior investigation of doubly fed induction generators with regard to rotor and grid-filter control strategies.

The dynamic and transient studies of the DFIG-based wind turbines have been carried out by various authors that can be categorized in several groups, such as impact of DFIG on power system dynamics, grid fault response of DFIG, low voltage ride-through (LVRT) capability enhancement of DFIG, participation of DFIG in grid frequency regulation, and investigation of DFIG dynamic behavior.

In [4–10], the impact of DFIG on the power system electromechanical oscillations has been studied. In [4–5], small signal stability of power system with DFIG is investigated. The impact of grid connected wind farms on power system oscillations is reviewed in [6]. In [7,8], the DFIG contributes to the network oscillation damping with using evolutionary techniques. In [9], the DFIG enhances the power system damping via network auxiliary power system stabilizer loop. The effect of DFIG on transient stability margin of synchronous generator is assessed by [10].

Some researches have been carried out addressing the grid fault response and short circuit current of DFIG [11–16]. These papers mainly consider the short circuit behavior of the DFIG, and develop theoretical analyses of the short circuit current.

In [17–20], the LVRT capability of the DFIG has been investigated in order to limit the rotor fault current and dc-link over voltage within their acceptable ranges during the grid voltage dip. By improving the LVRT capability, the DFIG remains connected to the grid during and after clearing the fault, and contributes to the system stability.

Participation of the DFIG in the power system frequency regulation has been studied in [21–23]. Therefore, DFIG can contribute to the grid stability enhancement by frequency regulation.

Various researchers have dealt with the dynamic behavior of the DFIG wind turbines [24–33]. In [24], dynamic performance of fixed speed wind turbine and DFIG is compared during power system disturbances. Transient stability of the DFIG due to short circuit fault is studied by [25]. The DFIG torsional oscillations due to wind turbine drive train dynamics are presented in [26–28]. In the dynamic studies of [29–30] the stator dynamics are not taken into account, and in [31–32] the dynamics of controllers are not considered. Also, in [33] there is no discussion about the critical modes and their effects on system dynamics.

The nature of transient instability, factors influencing it, mode of instability and the effects of system and controller parameters on DFIG dynamic behavior are not very clear in time domain DFIG related literatures. Also, little work has been carried out regarding poorly damped modes of DFIG, and their effects on DFIG dynamic performance.

The aim of this paper is to provide insight about the dynamic behavior of DFIG based wind turbines. Controller parameters of the DFIG have an important impact on the dynamic performance of the wind turbine. Therefore DFIG controllers will play a significant role in the future power system with increased penetration of DFIG. The paper considers generic PI controllers for regulation of rotor and grid-filter currents, and investigates the impacts of rotor and grid-filter controller parameters on the DFIG dynamic performance under voltage dips.

The structure of the paper is as follows. Following this introduction, dynamic model of the DFIG is given. Then, modal analysis of the system is presented. Based on this analysis, poorly damped modes of the system are extracted and the effects of these modes on the DFIG dynamic performance are examined both analytically and by simulations. Also, transient behavior of the DFIG with regard to different control parameters is examined.

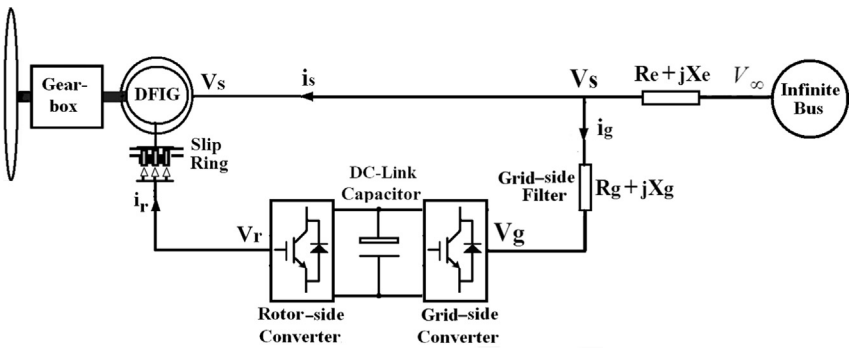

Fig. 1. DFIG connected to the infinite bus.

List of symbols

V_∞	voltage amplitude of infinite bus
ψ_{sdq} , ψ_{rdq}	dq components of stator and rotor fluxs
i_{rdq}, i_{sdq} ,i_{gdq}	dq components of rotor, stator and grid-filter currents
v_{rdq}, v_{sdq} ,v_{gdq}	dq components of rotor, stator and grid-filter voltages
$i_{rdq-ref}$, $i_{gdq-ref}$	dq components of rotor and grid-filter reference currents
P_e	DFIG electrical real power
ω_b	base angular frequency (in rad/s)
ω_s , ω_r	synchronous and rotor angular frequency (in pu)
ω	angular frequency of stator flux vector (in pu)
s , ω_2	rotor slip and rotor slip frequency
L_s , L_r	stator and rotor self inductances
R_s , R_r	stator and rotor resistances
L_m	magnetizing inductance
s , r	first subscript indicates stator and rotor
d , q	second subscript indicates direct and quadrature axes
0	subscript corresponding to operating point quantities
g	first subscript indicates grid-side filter

2. DFIG-based wind turbine modeling in stator flux orientation

The purpose of this section is to present the dynamic model of single machine infinite bus (SMIB) system of Fig. 1 in synchronous reference frame with the stator flux orientation. The discussion considers generic PI controllers for regulation of rotor and grid-filter currents, rotor speed and reactive power. The generalized machine model is developed based on the following conditions and assumptions:

(a) Positive direction for the stator and rotor currents is assumed into the generator (see Fig. 1).
(b) The equations are derived in synchronous reference frame using direct (d) and quadrature (q) axes representation.
(c) All system parameters and variables are in per unit and referred to the stator side of DFIG.

The stator and rotor voltages and fluxes, electromechanical torque, and reactive power injected to the grid by the DFIG, in the reference frame rotating at angular speed of ω, are given by [17]:

$$v_{sdq} = R_s i_{sdq} + j\omega\psi_{sdq} + \frac{1}{\omega_b}\frac{d\psi_{sdq}}{dt} \tag{1}$$

$$v_{rdq} = R_r i_{rdq} + j\omega_2\psi_{rdq} + \frac{1}{\omega_b}\frac{d\psi_{rdq}}{dt} \tag{2}$$

$$\psi_{sd} = L_s i_{sd} + L_m i_{rd} \quad \psi_{sq} = L_s i_{sq} + L_m i_{rq} \tag{3}$$

$$\psi_{rd} = L_m i_{sd} + L_r i_{rd} \quad \psi_{rq} = L_m i_{sq} + L_r i_{rq} \tag{4}$$

$$T_e = \frac{L_m}{L_s}(\psi_{sq} i_{rd} - \psi_{sd} i_{rq}) \tag{5}$$

$$Q_s = v_{sd}.i_{sq} - v_{sq}.i_{sd} \tag{6}$$

2.1. Rotor modeling

From (2) to (4), the rotor dynamics is described in terms of rotor current and stator flux, as follows:

$$\frac{L'_r}{\omega_b}\frac{di_{rdq}}{dt} = -R'_r i_{rdq} - j\omega_2 L'_r i_{rdq} - E_{dq} + v_{rdq} \tag{7}$$

where, $L'_r = L_r - \frac{L_m^2}{L_s}$, $R'_r = R_r + \left(\frac{L_m}{L_s}\right)^2 R_s$, and

$$E_{dq} = \frac{L_m}{L_s}\left(v_{sdq} - j\omega_r\psi_{sdq} - \frac{R_s}{L_s}\psi_{sdq}\right) \tag{8}$$

E_d and E_q in (8) are functions of stator flux and stator voltage. These terms, called rotor back-emf voltages, reflect the effects of stator dynamics on rotor current dynamics and have an important role on DFIG transient performance. By compensating the cross coupling terms, $\omega_2 L'_r i_{rq}$ and $-\omega_2 L'_r i_{rd}$, by $d-q$ rotor current controllers, the d and q rotor current control loops will be decoupled.

In order to decrease tracking error, the back-emf voltages, E_d and E_q, can be compensated by rotor current controllers using feed forward terms. Considering the rotor controllers to be PI, $K_{Idq}(s) = k_{p-idq} + k_{i-idq}/s$, and under compensation of cross coupling terms, the $d-q$ rotor voltage could be stated as

$$v_{rdq}(t) = k_{p-idq}.(i_{rdq-ref}(t) - i_{rdq}(t)) + k_{i-idq}.\int (i_{rdq-ref}(t) - i_{rdq}(t))dt + j\omega_2 L'_r i_{rdq} + k_{r-com}.E_{dq}(t) \tag{9}$$

Considering (9) as the rotor control voltage, the rotor $d-q$ current control loops can be described by Fig. 2(a). In this figure, the back-emf voltages, E_d and E_q, are represented as disturbances. In (9) and Fig. 2(a), k_{r-com} is either 0 or 1. $k_{r-com}=1$ means that back-emf voltages are compensated by rotor current controllers, and $k_{r-com}=0$ means that they are not compensated. Considering Fig. 2(a), the open loop bandwidth of current control in per unit is $\alpha_s = R'_r/L'_r$, which is relatively small. By pole cancellation of the plant with the zero of controller, in Fig. 2(a), we have

$$\frac{k_{i-idq}}{k_{p-idq}} = \frac{R'_r}{L'_r}\omega_b \tag{10}$$

Selecting, $k_{p-idq} = \alpha_{dq} L'_r/\omega_b$, and by taking (10) into account, the transfer function from $i_{rdq-ref}$ to i_{rdq} will be

$$G_{cl-idq} = \frac{I_{dq}(s)}{I_{dq-ref(S)}} = \frac{\alpha_{dq}}{s+\alpha_{dq}} \tag{11}$$

α_{dq} is the closed loop bandwidth of $d-q$ rotor current control, $\alpha_{dq} = (k_{p-idq}/L'_r)\omega_b$. Also, the transfer function from E_{dq} to i_{rdq} is given by:

$$\frac{I_{rdq}(s)}{E_{dq(S)}} = -\frac{\omega_b}{L'_r}\frac{s}{(s+\alpha_{dq})(s+\alpha_s)} \tag{12}$$

Normally, α_s is small and therefore the rotor current response to back-emf voltages is relatively slow. To overcome this problem, the open loop bandwidth, α_s, can actively be increased by means of control, this is called active damping. The current control loop with active damping is depicted in Fig. 2(b). Considering Fig. 2(b), the improved open loop bandwidth will be $\alpha_{s-active} = (R'_r + R_{r-active}/L'_r)\omega_b$. From (7) and (9) and Fig. 2(b), the rotor current dynamics can be presented as

$$\frac{L'_r}{\omega_b}\frac{di_{rd}}{dt} = -R'_r i_{rd} + (k_{r-com}-1)E_d + k_{p-id}(i_{rd-ref} - i_{rd}) + x_5 - R_{r-active} i_{rd} \tag{13}$$

$$\frac{L'_r}{\omega_b}\frac{di_{rq}}{dt} = -R'_r i_{rq} + (k_{r-com}-1)E_q + k_{p-iq}(i_{rq-ref} - i_{rq}) + x_6 - R_{r-active} i_{rq} \tag{14}$$

$$\frac{dx_5}{dt} = k_{i-id}(i_{rd-ref} - i_{rd}) \tag{15}$$

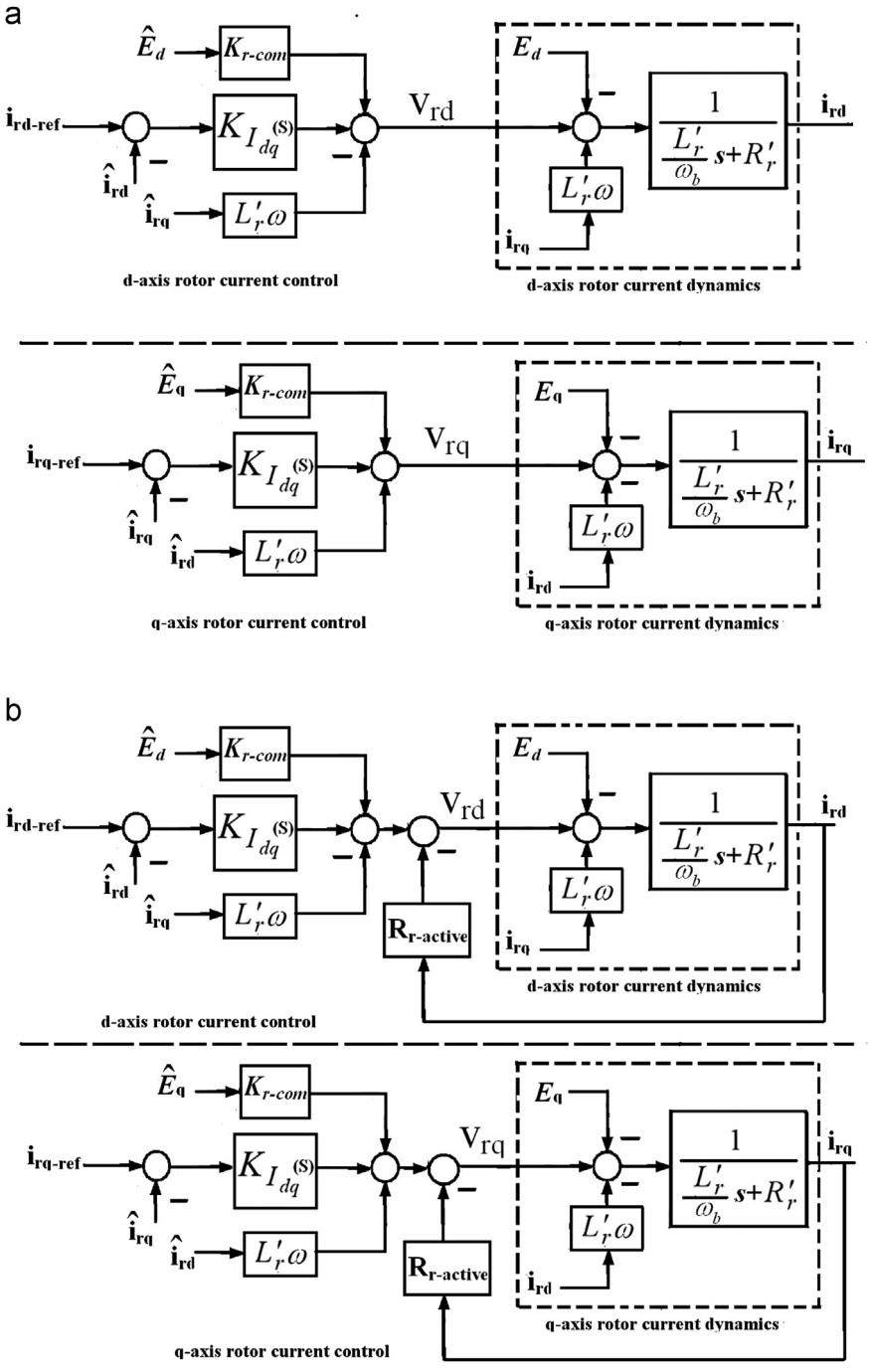

Fig. 2. (a) Rotor current control loop, (b) rotor current control loop with active damping.

$$\frac{dx_6}{dt} = k_{i-iq}(i_{rq-ref} - i_{rq}) \tag{16}$$

$R_{r-active}$ is the rotor active resistance caused by active damping shown in Fig. 2(b).

2.2. Grid-side filter modeling

The grid-side filter, as shown in Fig. 1, consists of inductance L_g and resistance R_g, and its dynamics are described by:

$$\frac{L_g}{\omega_b}\frac{di_{gdq}}{dt} = -R_g i_{gdq} - j\omega L_g i_{gdq} - v_{gdq} + v_{sdq} \tag{17}$$

where v_{sdq}, i_{gdq} and v_{gdq} are $d-q$ components of the generator terminal voltage and grid-side filter current and voltage, respectively. v_g is provided by the grid-side converter. By compensating the cross coupling terms, $\omega L_g i_{gq}$ and $-\omega L_g i_{gd}$, the d and q grid-filter current control loops will be decoupled. Fig. 3 depicts the $d-q$ grid-filter current control loops. The voltages v_{sd} and v_{sq}, in Fig. 3, are represented as disturbances in the current control loops. In order to decrease tracking error, these voltages can be compensated using feed forward terms.

Considering Fig. 3 and assuming the grid-filter current controller to be PI, $K_{G_{dq}}(s) = k_{p-g} + k_{i-g}/s$, the $d-q$ grid-filter voltage, under compensation of cross coupling terms, could be stated as

$$v_{gdq}(t) = -k_{p-g}(i_{gdq-ref}(t) - i_{gdq}(t)) - k_{i-g}\int (i_{gdq-ref}(t) - i_{gdq}(t))dt - j\omega L_g i_{gdq} + k_{g-com} v_{sdq}(t) \tag{18}$$

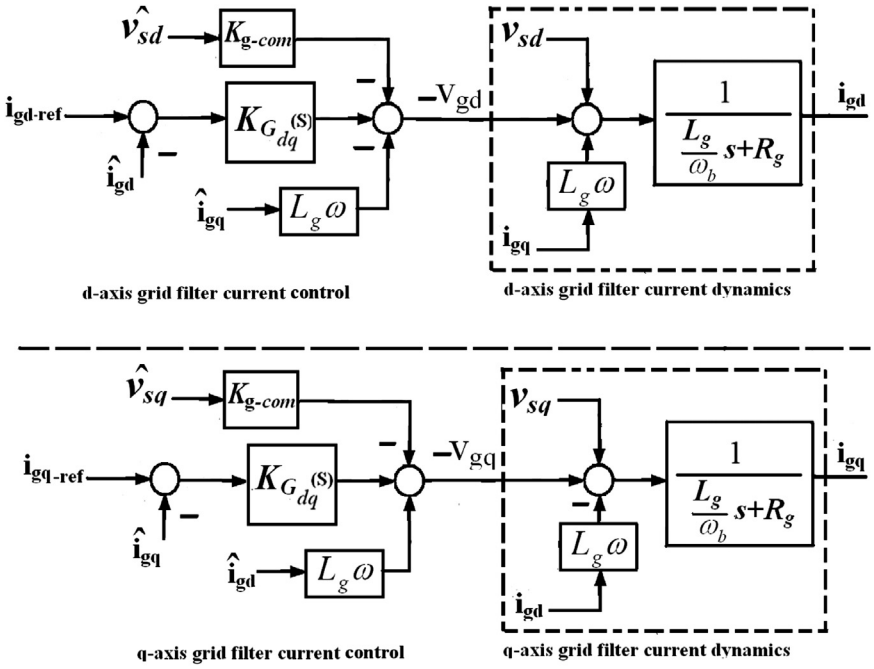

Fig. 3. Grid-side filter current control loop.

In (18), $k_{g-com}=1$ means that back-emf voltages are compensated by the rotor current controllers, and $k_{g-com}=0$ means that they are not compensated. From (17) and (18), the grid-side filter dynamics can be presented as

$$\frac{L_g}{\omega_b}\frac{di_{gd}}{dt}=-R_g i_{gd}+k_{p-g}(i_{gd-ref}-i_{gd})+x_{14}+(1-k_{g-com})v_{sd} \tag{19}$$

$$\frac{L_g}{\omega_b}\frac{di_{gq}}{dt}=-R_g i_{gq}+k_{p-g}(i_{gq-ref}-i_{gq})+x_{15}+(1-k_{g-com})v_{sq} \tag{20}$$

$$\frac{dx_{14}}{dt}=k_{i-g}(i_{gd-ref}-i_{gd}) \tag{21}$$

$$\frac{dx_{15}}{dt}=k_{i-g}(i_{gq-ref}-i_{gq}) \tag{22}$$

The PI controller parameters of rotor and grid-filter current controls, in (9) and (18), are selected such that the closed-loop bandwidths of the control loops, in Figs. 2 and 3, are identical.

2.3. Stator modeling

In stator flux orientation, $\psi_s=\psi_{sd}$ and $\psi_{sq}=0$. Then, from (1), (3) and (4), the stator can be described by the following state equations as a function of rotor current, stator flux, and infinite bus voltage.

$$\frac{1}{\omega_b}\frac{L_s+L_e}{L_s}\frac{d\psi_{sd}}{dt}=-\frac{R_s+R_e}{L_s}\psi_{sd}+\frac{R_s+R_e}{L_s}L_m i_{rd}-R_e i_{gd}$$
$$-\frac{L_e L_m}{L_s}\omega i_{rq}+L_e\omega i_{gq}+\frac{L_e L_m}{L_s}\frac{1}{\omega_b}\frac{di_{rd}}{dt}-\frac{L_e}{\omega_b}\frac{di_{gd}}{dt}+V_\infty\cos\gamma \tag{23}$$

$$\frac{d\gamma}{dt}=\omega_b(\omega_s-\omega) \tag{24}$$

and,

$$\omega=\frac{R_s+R_e}{L_s}L_m i_{rq}-R_e\frac{i_{gq}+\frac{L_e L_m}{L_s}\frac{1}{\omega_b}\frac{di_{rq}}{dt}-\frac{L_e}{\omega_b}\frac{di_{gq}}{dt}+V_\infty\sin\gamma}{\psi_{sd}\left(1+\frac{L_e}{L_s}\right)-\frac{L_e}{L_s}L_m i_{rd}+L_e i_{gd}} \tag{25}$$

where, $\omega_s=(1/\omega_b)(d\theta_s/dt)$ and $\omega=(1/\omega_b)(d\theta/dt)$. θ_s and θ are the infinite bus voltage angle and stator flux angle in stationary reference frame, respectively. Also, γ is the difference between θ_s and θ.

2.4. Drive train model and speed controller

The drive train comprises turbine, gear box, shafts and other mechanical components of wind turbine. A multi mass (usually two mass) model must be used for dynamic/transient studies of wind turbines with DFIG. The two mass model is given by [31].

$$\frac{d\omega_r}{dt}=\frac{T_e+k_s\beta+D(\omega_t-\omega_r)}{2H_r} \tag{26}$$

$$\frac{d\omega_t}{dt}=\frac{T_m-k_s\beta-D(\omega_t-\omega_r)}{2H_t} \tag{27}$$

$$\frac{d\beta}{dt}=\omega_b(\omega_t-\omega_r) \tag{28}$$

where ω_t and ω_r are the turbine and generator speeds in (pu), β is the shaft twist angle in (rad), H_r and H_t are the inertia constants of turbine and generator in (s), respectively, k_s is the shaft stiffness coefficient in (pu/elec. rad), D is the damping coefficient in (pu), T_e and T_m are the generator electrical torque and the turbine mechanical torque, respectively, in (pu). With stator flux orientation, the rotor speed is controlled by the q-components of rotor voltage and current, v_{rq} and i_{rq} [1]. The control scheme used for speed control is shown in Fig. 4. In this figure, α_q is the bandwidth of the q-axis rotor current control loop, and $T_{dis}=k_s\theta+D\omega_t$. Employing a PI controller for the speed controller, $K_\omega(s)=k_{p\omega}+k_{I\omega}/s$, state equation of the speed controller is

$$\frac{dx_7}{dt}=k_{I\omega}(\omega_{r-ref}-\omega_r) \tag{29}$$

The q-axis rotor current reference, for speed control and damping of rotor oscillations is

$$i_{rq-ref}=-k_{p\omega}(\omega_{r-ref}-\omega_r)-x_7 \tag{30}$$

2.5. Reactive power control

With stator flux orientation, terminal voltage and reactive power exchange between the generator and the grid can be controlled by the d-components of rotor voltage and current [1]. According to (6), in vector control with stator flux orientation, the

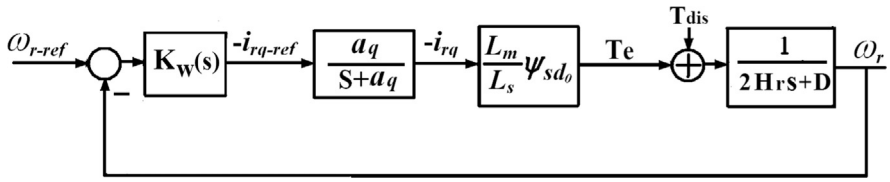

Fig. 4. Speed control loop.

Table 1
Stator power factor as a function of d-axis rotor current.

i_{rd0}(pu)	0	0.0862	0.172	0.345	0.52	0.69	0.862
Power factor	0.94 lag	0.96 lag	0.984 lag	1	0.98 lead	0.92 lead	0.879 lead

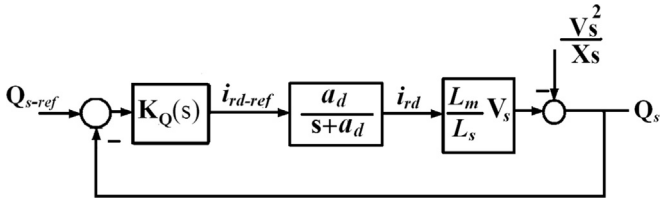

Fig. 5. Reactive power control loop.

reactive power injected to the grid by the stator, Q_s, can be written as

$$Q_s = \frac{1}{L_s \omega_s} \psi_{sd}(L_m i_{rd} - \psi_{sd}) \tag{31}$$

As can be seen, there is direct relation between d-axis rotor current and stator reactive power and the generator power factor. Table 1 shows the stator power factor with different d-axis rotor currents, for DFIG system of Appendix A.

Thus, the d-axis rotor reference current is determined by reactive power controller, as shown in Fig. 5. α_d in Fig. 5 is the bandwidth of the d-axis rotor current control loop. Using the PI controller as $K_Q(s) = k_{p-Q} + k_{I-Q}/s$, the state equation of the reactive power controller is

$$\frac{dx_8}{dt} = k_{I-Q}(Q_{s-ref} - Q_s) \tag{32}$$

The d-axis rotor current reference, for reactive power control is

$$i_{rd-ref} = k_{p-Q}(Q_{s-ref} - Q_s) + x_8 \tag{33}$$

3. Small signal stability and modal analysis

Eqs. (13)–(16), (19)–(30) and (32),(33) describe the dynamics of turbine-generator and rotor speed and reactive power controllers. The dynamic model of the DFIG wind turbine may be given by

$$x^{\bullet} = f(x, z, d)$$
$$0 = g(x, z, d) \tag{34}$$

where x, z and d are the vectors of the DFIG state variables, reference inputs and exogenous inputs, respectively, i.e.,

$$x = [\psi_{sd}, \gamma, i_{rd}, i_{rq}, x_5, x_6, i_{gd}, i_{gq}, x_{14}, x_{15}, x_7, x_8, \omega_r, \theta, \omega_t]^T,$$
$$z = [\omega_{r-ref}, Q_{s-ref}]^T, \quad d = [v_\infty, T_m]$$

Table 2
The sample DFIG system modes and dominant state variables.

System modes		State variables with highest participation factors	
$\lambda_{1,2}$	$-7.03 \pm j328.8$	ψ_{sd}	γ
λ_3	-755.6	i_{rd}	i_{rq}
λ_4	-735.6	i_{rq}	i_{rd}
$\lambda_{5,6}$	$-4 \pm j12.69$	ω_r	β
λ_7	-4.54	x_8	–
$\lambda_{8,9}$	$-0.57 \pm j1.56$	x_7	ω_t
λ_{10}	-13.27	x_5	–
λ_{11}	-14.7	x_6	–
$\lambda_{12,13}$	-754	i_{gd}	i_{gq}
$\lambda_{14,15}$	-3.63	x_{14}	x_{15}

Linearizing and rearranging (34) yields the linearized model of the DFIG-based wind turbine as follows.

$$\Delta x^{\bullet} = A.\Delta x + B.\Delta u \tag{35}$$

3.1. Modal analysis without compensation of rotor and grid-filter back-emf voltages

Modal analysis is carried out on the SMIB system shown in Fig. 1. Appendix A gives the parameters (in per unit) of the 1.66 MVA, 575 V, 60 Hz DFIG used for the study. The study is done under operating conditions of Appendix B. These conditions correspond to unity power factor at the stator terminal. The PI controller parameters are given in Appendix C. These parameters correspond to the rotor and grid-side filter current control bandwidths of 2 per unit (754 rad/s), speed control loop bandwidth of 4.4 rad/s (0.7 Hz) including active damping, and reactive power control loop bandwidth of 4.4 rad/s (0.7 Hz). Also, the grid impedance is assumed to be $R_e + jX_e = 0.01 + j0.1$. Table 2 shows the system modes and corresponding state variables with the highest participation factors under condition that rotor back-emf voltages are not compensated, i.e. with $k_{r-com} = 0$ in (13) and (14). Using the participation factors [34], the contribution degree of each state variable in the system modes and the physical nature of dynamic modes can be detected (see Appendix D). Considering Table 2, the following key points are found:

1. The dynamics of DFIG contain poorly damped modes ($-7.03 \pm j328.8$) with a corresponding natural frequency close to the network frequency. Stator variables, ψ_{sd} and γ, have the highest contribution in these modes, and consequently they represent the stator modes. As will be shown later, these modes have significant impact on transient performance of

DFIG, and under special operating conditions may become unstable.

2. The modes $\lambda_3 = -755.6$ and $\lambda_4 = -735.6$ are the $d-q$ rotor current modes, and i_{rd} and i_{rq} have the highest participation in these modes. These modes are very fast and their damping is approximately equal to the rotor current control bandwidth (2 pu or 754 rad/s). Thus, the larger rotor current control bandwidth, the larger damping of rotor current modes.
3. The modes $\lambda_{5,6} = -4 \pm j12.69$ are the electromechanical modes. The mechanical variables ω_r and β have the highest contribution in these modes. The corresponding natural frequency is relatively 2 Hz.
4. The real mode $\lambda_7 = -4.54$ is associated with state variable x_8, see (32), and is equal to bandwidth of reactive power control loop.
5. The modes $\lambda_{8,9} = -0.56 \pm j1.56$ are the mechanical modes associated with the state variables x_7 and ω_t. These modes are approximately weak and are dependent on the speed control bandwidth and damping.
6. The modes $\lambda_{10} = -13.27$ and $\lambda_{11} = -14.7$ are the rotor electrical modes associated with state variables x_5 and x_6 (see (15) and (16)). These modes are equal to the $d-q$ rotor current open loop bandwidth, $\alpha_s = (R'_r/L'_r)\omega_b$.
7. The modes $\lambda_{12,13} = -754$ are the $d-q$ grid-side filter current modes associated with state variables i_{gd} and i_{gq}. These modes are very fast and their damping is approximately equal to the grid-filter current control bandwidth (2 pu or 754 rad/s).
8. The modes $\lambda_{14,15} = -3.63$ are the grid-side filter modes associated with state variables x_{14} and x_{15} (see (21) and (22)). These modes are equal to the grid-filter current open loop bandwidth, $\alpha_g = (R_g/L_g)\omega_b$.

As stated above, the stator modes are weakly damped, e.g. the damping ratio of stator modes in Table 2 is $\xi = 0.0213$. Usually in the literature, the stator dynamics are neglected. However, these modes could have significant effects on DFIG transient behavior.

In the following sensitivities of stator modes with respect to rotor and grid-filter control bandwidths, rotor active damping, rotor and grid-filter back-emf voltages and DFIG power factor are examined.

Table 3
The sample DFIG system modes with rotor and grid-filter closed loop bandwidths of 4 pu.

System modes		State variables with highest participation factor	
$\lambda_{1,2}$	$-2.1 \pm j330.2$	ψ_{sd}	γ
λ_3	-1498.5	i_{rd}	i_{rq}
λ_4	-1513.6	i_{rq}	i_{rd}
$\lambda_{5,6}$	$-3.9 \pm j12.9$	ω_r	β
λ_7	-4.4	x_8	–
$\lambda_{8,9}$	$-0.6 \pm j1.6$	x_7	ω_t
λ_{10}	-13.5	x_5	–
λ_{11}	-14.0	x_6	–
$\lambda_{12,13}$	-950.2	i_{gd}	i_{gq}
$\lambda_{14,15}$	$-3.7 \pm j0.3$	x_{14}	x_{15}

3.2. Stator mode sensitivity with respect to rotor and grid-filter current closed loop bandwidths

Normally, increasing the rotor and grid-filter closed loop bandwidths can improve the rotor current dynamics, decrease tracking error, limit the rotor current transients and improve the DFIG low voltage ride-through capability. Participation factors show that the stator modes are somewhat related to the rotor and grid-filter state variables. Table 3 shows the system modes under condition that rotor and grid-filter closed loop bandwidths are selected as 4 pu. Comparing Tables 2 and 3 shows that increasing the rotor and grid-filter closed loop bandwidths while keeping all other parameters constant, decreases the damping of stator modes. Fig. 6 shows the stator modes real part as a function of rotor and grid-filter closed loop bandwidths. Thus, varying the rotor/grid-filter control bandwidths causes significant changes in damping of stator modes.

Also, increasing the rotor resistance passively, i.e. increasing R'_r, or actively, i.e. increasing $R_{r-active}$ in Fig. 2(b), can decrease the stator modes damping. Table 4 shows the system modes and dominant state variables for rotor active damping term of $R_{r-active} = 0.16$. Modal analysis shows that for $R_{r-active} = 0.16$ pu, the stator modes become $-0.71 \pm j310$. Thus, including active damping in the rotor current control loop can significantly decrease the stator modes damping.

3.3. Stator mode sensitivity with respect to d-axis rotor current

As it is clear from Table 1, there is direct relation between d-axis rotor current and stator reactive power and consequently the generator power factor. Modal analysis shows that increasing the d-axis rotor current can decrease the damping of stator modes. Fig. 7 shows the real part of stator modes as a function of d-axis rotor current for two different values of rotor and grid-filter current closed loop bandwidths. Considering Fig. 7, it is clear that increasing the d-axis rotor current, while having large bandwidths of current control loops, can move the stator modes to unstable state and deteriorates the DFIG dynamic performance. In other words, moving the turbine-generator to leading power factor can influence the DFIG dynamic behavior.

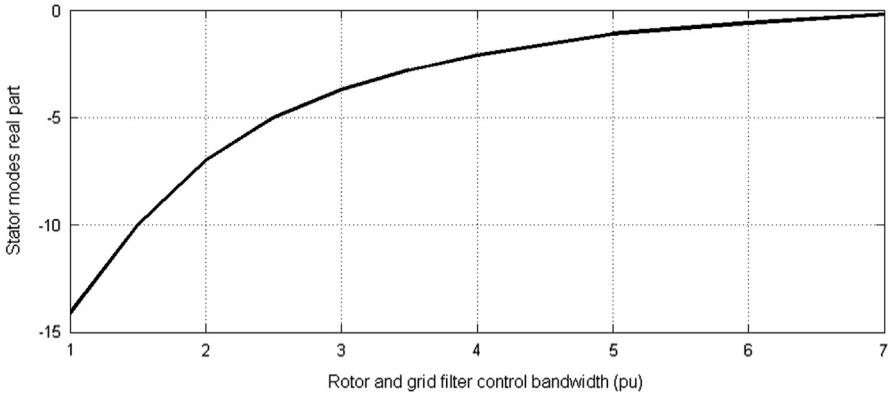

Fig. 6. Real part of the stator modes as a function of rotor and grid-filter closed loop bandwidths.

3.4. Modal analysis with compensation of rotor back-emf voltages

It is possible to include a feed forward compensating term in the control law to compensate for the tracking error caused by variations in the rotor back-emf voltages. Table 5 shows the system modes and dominant state variables after compensating of rotor and grid-filter back-emf voltages. Comparing Tables 2 and 5 shows that compensation of back-emf voltages can significantly decrease the damping of stator modes, but the other system modes remain constant. Therefore, although compensation of back-emf voltages can improve the DFIG low voltage ride-through capability and limit the peak value of rotor current transients, but it may decrease the stator modes damping.

$$-\frac{L_eL_m}{L_s}.\omega i_{rq-ref}+L_e\omega i_{gq-ref}+\frac{L_eL_m}{L_s}\frac{1}{\omega_b}\frac{di_{rd-ref}}{dt}-\frac{L_e}{\omega_b}\frac{di_{gd-ref}}{dt}+V_\infty\cos\gamma \tag{36}$$

$$\frac{d\gamma}{dt}=\omega_b.\left(\omega_s-\frac{(R_s+R_e/L_s)L_mi_{rq-ref}-R_{ei}^{gq-ref}+(L_eL_m/L_s)(1/\omega_b)(di_{rq-ref}/dt)-(L_e/\omega_b)(di_{gq-ref}/dt)+V_\infty sin\gamma}{\psi_{sd}(1+(L_e/L_s))-(L_e/L_s)L_mi_{rd-ref}+L_ei_{gd-ref}}\right) \tag{37}$$

4. Analysis of stator flux dynamics

If the current control loop of the rotor and grid-filter is fast enough, it is possible to decouple the flux dynamics from other system dynamics and set the rotor and grid-filter currents to their reference values. This means that to study the stator flux dynamics, it is sufficient to consider (36) and (37).

$$\frac{1}{\omega_b}\frac{L_s+L_e}{L_s}.\frac{d\psi_{sd}}{dt}=-\frac{R_s+R_e}{L_s}\psi_{sd}+\frac{R_s+R_e}{L_s}L_m.i_{rd-ref}-R_ei_{gd-ref}$$

The equilibrium points of these equations are γ_0 and $\psi_{sd0}\approx 1$. The linearized dynamic model of (36) and (37) around the operating point is obtained as

$$\begin{bmatrix}\Delta\psi_{sd}^{\bullet}\\ \Delta\gamma^{\bullet}\end{bmatrix}=\omega_b\begin{bmatrix}a_{11} & a_{12}\\ a_{21} & a_{22}\end{bmatrix}\begin{bmatrix}\Delta\psi_{sd}\\ \Delta\gamma\end{bmatrix} \tag{38}$$

in which a_{11} to a_{22} are given in Appendix E. According to Appendix E, the exact characteristics polynomial is given by

$$\lambda^2+\omega_b\left(\frac{R_s+R_e}{L_s+L_e}+\frac{(R_s+R_e/L_s)\psi_{sd0}-(R_s+R_e/L_s)L_mi_{rd0}+R_ei_{gd0}}{\psi_{sd0}(1+(L_e/L_s))-(L_eL_m/L_s)i_{rd0}+L_ei_{gd0}}\right)+\left(\frac{R_s+R_e}{L_s+L_e}\frac{v_{\infty d0}}{D}+\frac{v_{\infty q0}}{D}\right)\omega_b^2=0 \tag{39}$$

where $v_{\infty d0}=V_\infty\cos\gamma_0=\cos\gamma_0$, $v_{\infty q0}=V_\infty\sin\gamma_0$, and $D=\psi_{sd0}(1+(L_e/L_s))-(L_eL_m/L_s)i_{rd0}+L_ei_{gd0}$. For typical operating conditions, γ_0 is close to $(\pi/2)$, $L_m\cong L_s$ and $L_e\ll L_s$. Therefore, the simplified

Table 4
The sample DFIG system modes with rotor active damping term, $R_{r-active}=0.16$.

System modes		State variables with highest participation factors	
$\lambda_{1,2}$	$-0.71\pm j309.8$	ψ_{sd}	γ
λ_3	-755.98	i_{rd}	i_{rq}
λ_4	-730.8	i_{rq}	i_{rd}
$\lambda_{5,6}$	$-3.9\pm j13.05$	ω_r	β
λ_7	-4.43	x_8	–
$\lambda_{8,9}$	$-0.58\pm j1.58$	x_7	ω_t
$\lambda_{10,11}$	$-216.13\pm j21.55$	x_5	x_6
$\lambda_{12,13}$	$-474\pm j131.3$	i_{gd}	i_{gq}
$\lambda_{14,15}$	$-3.64\pm j0.53$	x_{14}	x_{15}

Table 5
The sample DFIG system modes with compensation of rotor and grid-filter back-emf voltages.

System modes		State variables with highest participation factors	
$\lambda_{1,2}$	$-0.41\pm j376$	ψ_{sd}	γ
λ_3	-758.4	i_{rd}	–
λ_4	-745.1	i_{rq}	–
$\lambda_{5,6}$	$-3.89\pm j13.11$	ω_r	β
λ_7	-4.37	x_8	–
$\lambda_{8,9}$	$-0.57\pm j1.56$	x_7	ω_t
$\lambda_{10,11}$	-13.41	x_5	x_6
$\lambda_{12,13}$	-753.98	i_{gd}	i_{gq}
$\lambda_{14,15}$	-3.77	x_{14}	x_{15}

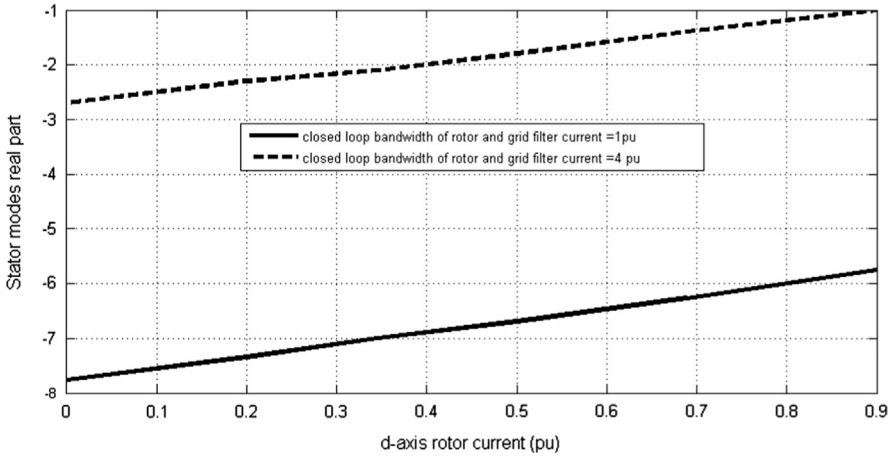

Fig. 7. Stator modes real part with respect to i_{rd} under different rotor and grid filter control bandwidths.

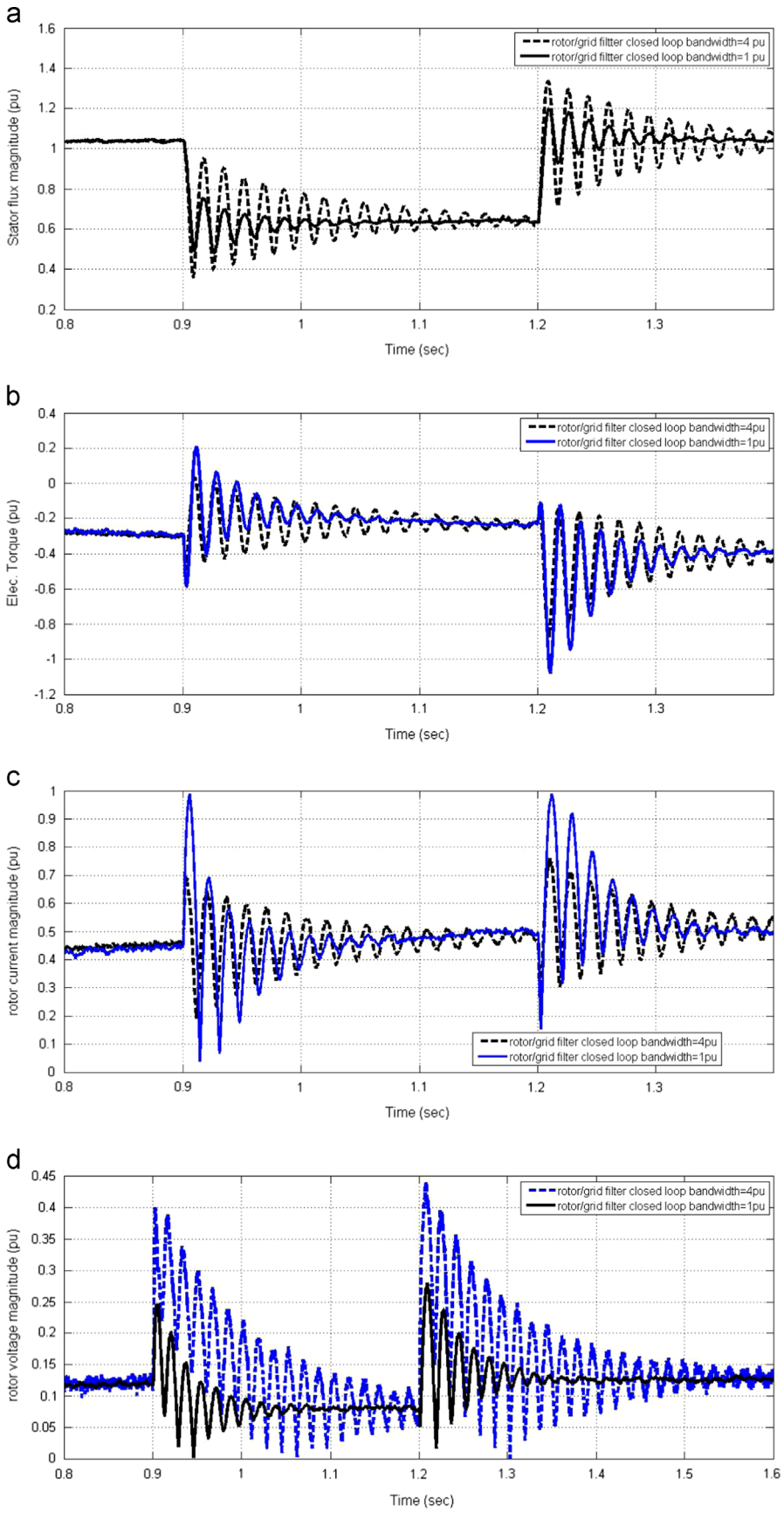

Fig. 8. Transient behavior of DFIG with two different values of rotor and grid filter control bandwidths, in pu, (a) stator flux magnitude, (b) electrical torque, (c) rotor current magnitude (d) rotor voltage magnitude.

characteristic polynomial is approximately found as

$$\lambda^2+\omega_b\left(\frac{R_s+R_e}{L_s+L_e}+\frac{(R_s+R_e/L_s)\psi_{sd0}-(R_s+R_e/L_s)L_m i_{rd0}+R_e i_{gd0}}{\psi_{sd0}(1+(L_e/L_s))-(L_eL_m/L_s)i_{rd0}+L_e i_{gd0}}\right)+\omega_b^2=0 \tag{40}$$

Considering (40), it is clear that the stator mode natural frequency is close to the line frequency, i.e., 1 pu. For maintaining stability of the (38), it is required that

$$i_{rd0}\left(1+\frac{L_e}{L_s+L_e}\right)-\frac{L_s}{L_m}i_{gd0}\left(\frac{L_e}{L_s+L_e}+\frac{R_e}{R_s+R_e}\right)<\frac{2\psi_{sd0}}{L_m} \tag{41}$$

If inequality (41) is satisfied, the nonlinear stator dynamics is locally asymptotically stable. In normal conditions, the grid-side converter operates at unity power factor, and consequently d-axis grid filter current, i_{gd0}, exchanging reactive power with the grid is equal to zero. Hence, by setting $i_{gd0}=0$ in (41), we have

$$i_{rd0}\left(1+\frac{L_e}{L_s+L_e}\right)<\frac{2\psi_{sd0}}{L_m} \tag{42}$$

Considering (42), it is clear that stator dynamics is dependent on operating condition, i_{rd0}, and correspondingly, stator power factor. Also, it depends on the network and generator parameters such as L_e and L_s.

5. Time domain simulations

In the previous section, modal analysis of the DFIG system was presented and the effects of different rotor and grid-filter control strategies on the poorly stator modes were investigated. The approximation of the DFIG dynamic and transient characteristics can be obtained from the eigenvalues of the linearized DFIG model presented in Section 3. In this section dynamic and transient behavior of the DFIG system is studied. The simulations are carried out on the SMIB system shown in Fig. 1. The system and controller parameters of the DFIG used in these studies are shown in Appendix A and C. The DFIG operating slip and electrical power before the fault are $s_0=-0.1$ and $P_{e0}=0.5\,pu$, respectively, and the generator is operated at unity power factor. The grid impedance is assumed to be $R_e+jX_e=0.05+j0.5$.

5.1. Effects of rotor and grid-filter closed loop bandwidths

To find out the effects of the rotor and grid-filter closed loop bandwidths on the DFIG transient behavior, a 40% voltage dip with duration of 300 ms is imposed on the DFIG terminal at $t=0.9$ s. Fig. 8 shows the transient response of the DFIG with two different values of rotor and grid-filter closed-loop bandwidths. Considering Fig. 8, increasing the closed loop bandwidth from 1 pu to 4 pu limits the peak value of rotor current, electrical torque and stator flux, but it results in oscillatory transient response with larger settling time. This is because as stated in Section 3, the stator flux and thus the DFIG transient response is less damped with higher rotor and grid-filter closed loop bandwidths. Moreover, it is clear from Fig. 8 that the larger closed loop bandwidth, the larger control efforts and rotor voltages (v_{rd} and v_{rq}). Therefore, a trade off is needed between the transient response settling time, peak value of transient responses and control effort, in selection of appropriate rotor and grid-filter closed loop bandwidths.

5.2. Effects of rotor active damping

As already mentioned in Section 3.2, including active damping in the rotor current control loop, the term $R_{r-active}$ in Fig. 2(b) can significantly weaken the stator dynamics. To demonstrate the impact of rotor active damping on the DFIG transient behavior, a 50% voltage dip with duration of 300 ms is imposed on the DFIG terminal at $t=0.9$ s. Fig. 9 shows the transient response of the DFIG with and without rotor current active damping for $R_{r-active}=0.2$ and $R_{r-active}=0$. It is clear from Fig. 9 that the DFIG stability margin in the case with the rotor active damping is lower than that of the case without active damping.

Therefore, the settling time and oscillations of transient responses in the case with $R_{r-active}=0.2$ are much higher than that of the case with $R_{r-active}=0$. This is because the stator flux and thus the DFIG transient response is less damped with higher rotor resistance. Hence, increasing the rotor active damping cannot improve the DFIG low voltage ride-through capability. This in turn can deteriorate the DFIG transient performance, i.e. larger oscillations in stator flux, electrical torque, terminal voltage, and rotor currents.

5.3. Effects of rotor back-emf voltages

To find out the effects of compensation of rotor back-emf voltages on the DFIG transient behavior, a simulation is carried out for a 50% voltage dip with duration of 300 ms. In this simulation (Fig. 10) two states are considered. In the first state the back-emf voltages are not compensated, and in the second state they are compensated. It is clear from Fig. 10 that compensation of these voltages limits the peak value of the rotor current transients, but it decreases the DFIG stability margin. Therefore, by compensating of back-emf voltages, the settling time and oscillations of stator flux and electrical torque are increased. Moreover, this state requires larger rotor voltages and control efforts.

5.4. Transient stability study

As stated in Section 4 and considering (42), the stability of stator dynamics is closely related to the network reactance, L_e. To demonstrate the prominent role of stator dynamics on the DFIG transient performance, a 70% voltage dip with duration of 300 ms is imposed on the infinite bus at $t=0.9$ s. In this simulation, Fig. 11, two different network impedances are considered. In the first case $R_e+jX_e=0.05+j0.3$pu, and in the second case, $R_e+jX_e=0.05+j0.5$pu. In both cases, the slip and real power of the system at the equilibrium point are -0.1 and 0.5 pu.

It is clear from Fig. 11 that in case 2 with higher network reactance, the stator flux at the time of clearing the fault is out of the stator domain of attraction, and consequently, stator state trajectories do not reach their stable post fault operating point and transient behavior of the DFIG is unstable. The final outcome of transient instability is large oscillations in the terminal voltage, electrical torque and rotor speed of DFIG.

In wind turbine-generators, the nature of instability is different from the rotor angle instability of conventional synchronous generators. In the wind turbines with the DFIG the generator speed range is approximately $\pm 30\%$ around the synchronous speed. The upper limit of the generator speed is determined by the back-to-back converter capacity rating. If the generator speed after clearing the fault is higher than the limit, the converter cannot handle the slip power and the generator may become unstable. For the DFIG system studied in this paper the operating speed before the fault is 1.1 pu and the generator speed at the moment of clearing the fault (at $t=1.2$ s) is 1.11 pu. Thus, the generator slip after the fault is within the allowable range and the back-to-back converter is able to handle the slip power. Moreover, growth of the generator speed during the fault is relatively low. Therefore, the system does not face angle/speed instability. In the second case, in spite of admissible slip, the system experiences instability that roots in the stator dynamics and exhibits as transient voltage instability.

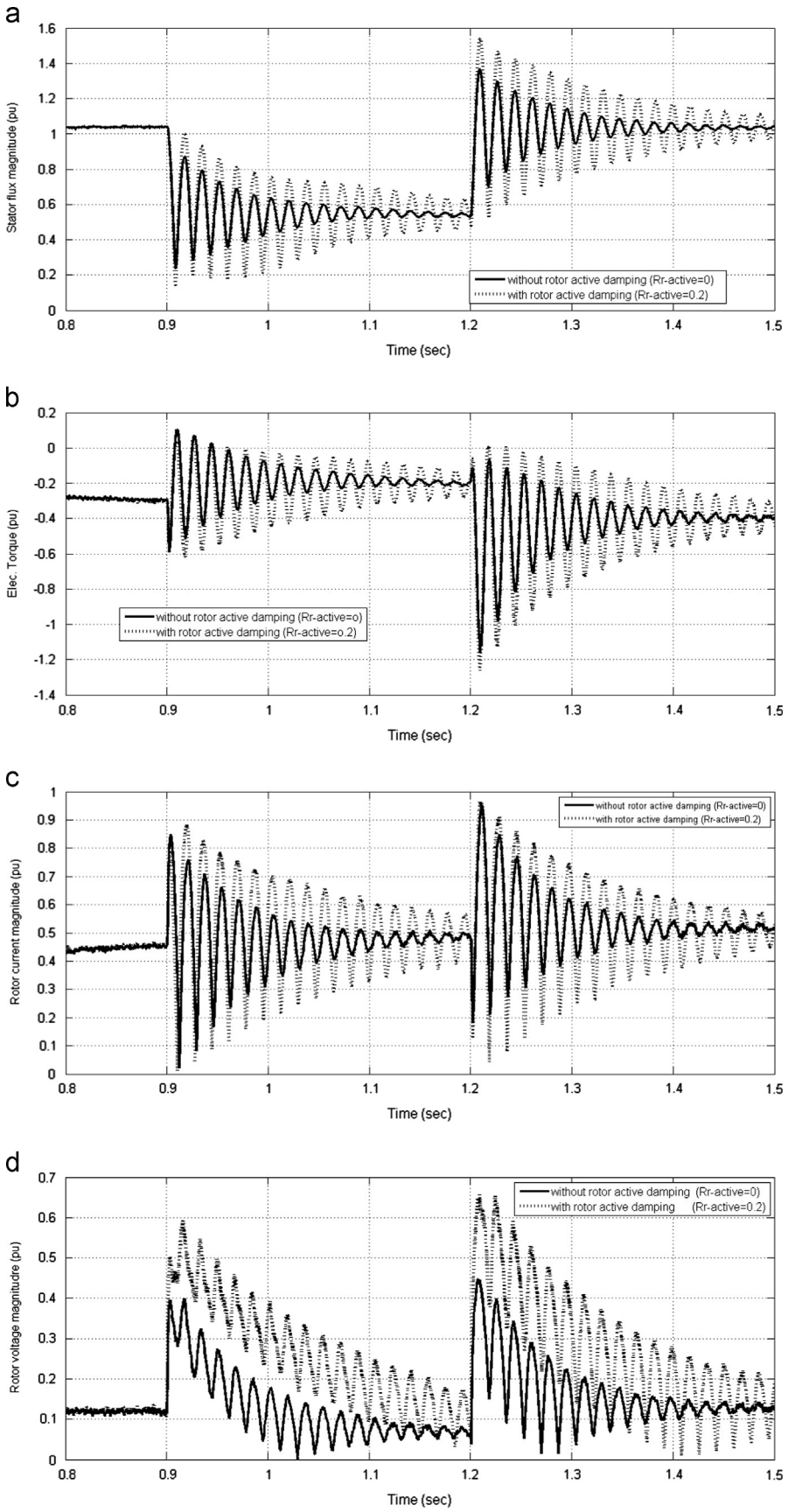

Fig. 9. Transient behavior of DFIG with and without rotor active damping, $R_{r-active}=0$ and $R_{r-active}=0.2$, in pu, (a) stator flux magnitude, (b) electrical torque, (c) rotor current magnitude, (d) rotor voltage magnitude.

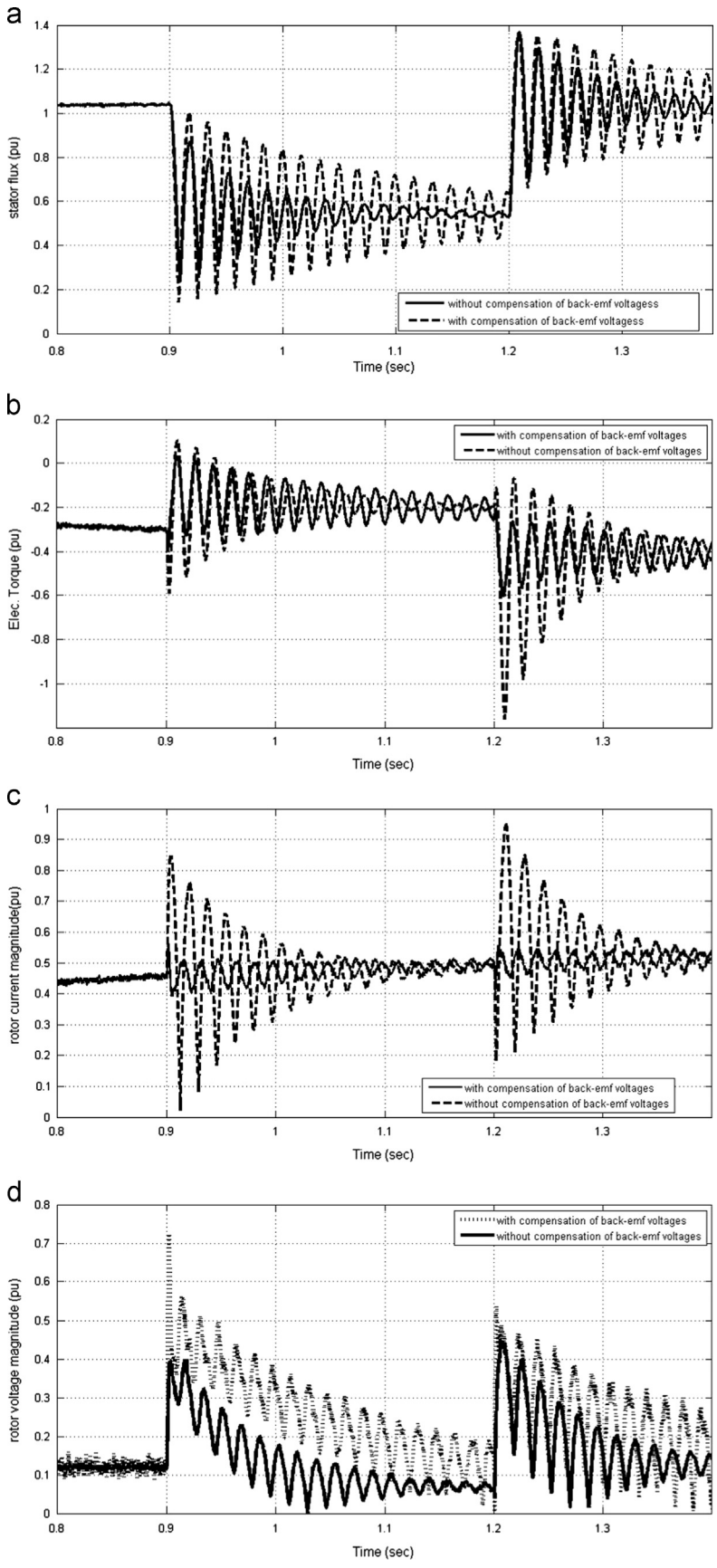

Fig. 10. Transient behavior of DFIG with and without compensation of back-emf voltages, in pu, (a) stator flux, (b) electrical torque, (c) rotor current magnitude, (d) rotor voltage magnitude.

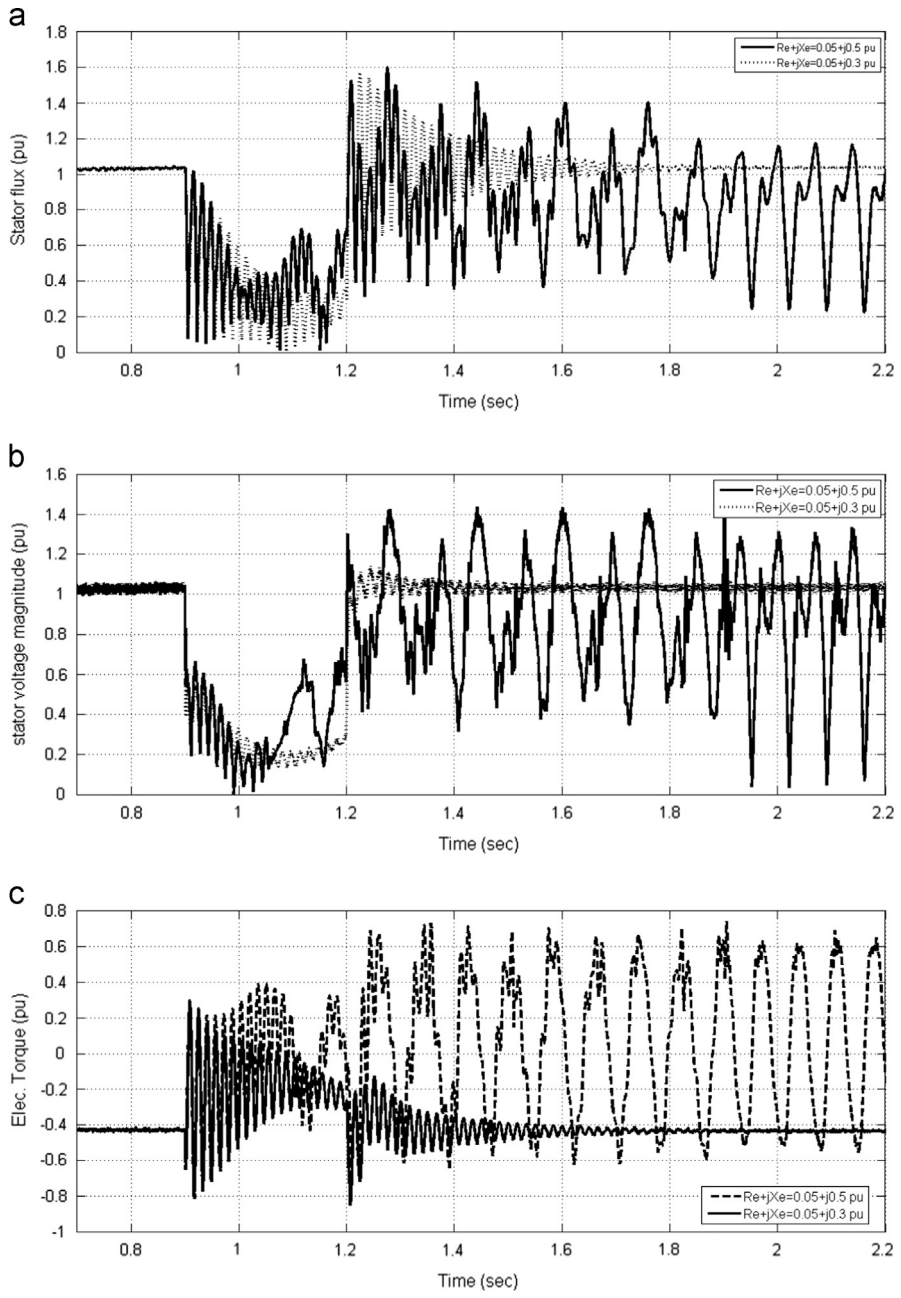

Fig. 11. DFIG transient response under 300 ms voltage dip, with two different values of network reactance ($R_e+jX_e=0.05+j0.3$pu and $R_e+jX_e=0.05+j0.5$pu), in pu, (a) stator flux magnitude (ψ_{sd}), (b) terminal voltage magnitude, (c) electrical torque.

6. Conclusion

This paper studied the dynamic and transient behavior of wind turbine with DFIG with regard to rotor and grid-filter control strategies. The investigations include modal and sensitivity analysis, stator dynamics analysis, and time domain simulations. The discussion considered generic PI controllers for the regulation of rotor and grid-filter currents, rotor speed and reactive power. It was shown that the dynamics of the DFIG contain poorly damped modes corresponding to stator modes. Also, it was found that the rotor back-emf voltages, closed loop bandwidths of rotor and grid-filter currents, and rotor current active damping have high impacts on the stator modes and thus on the DFIG dynamic performance. The approximation of the DFIG dynamic and transient behavior can be obtained from the modal analysis and eigenvalues of the linearized DFIG model.

The paper results show that the dynamic behavior of the DFIG under voltage dips is strongly affected by the stator dynamics. Increasing the rotor and grid-filter closed loop bandwidths and compensation of back-emf voltages can improve the rotor and grid-filter dynamics, decrease tracking error and limit the rotor current transients. At the same time, they can lead to poorly stator modes and deteriorate the DFIG transient performance. Also, including active damping term in the rotor current control loop can decrease the DFIG stability margin with less damped transient response. Therefore, the dynamic performance of the DFIG is to a large extent dependent on rotor controller parameters.

In the near future wind farms will be vital and important sections of the power system generation. Hence, control strategies of the DFIG and consequently wind farm will influence on the future power system operation. Also, they will play a significant

role in order to guarantee stable and secure operation in the near future with increased wind power penetration.

Appendix A. Parameters of the 1.66 MVA, 575 V, 60 Hz, DFIG-based wind turbine:

$V_{base} = 575$ V, $S_{base} = 1.66$ MVA
$f_{base} = 60$ Hz, $\omega_b = 2\pi f_{base} = 377$ rad/s, $R_s = 0.00706$ pu
$R_r = 0.005$ pu, $L_s = 3.07$ pu, $L_r = 3.056$ pu, $L_m = 2.9$ pu
$L_g = 0.3$ pu, $R_g = 0.003$ pu
$H_r = 0.75$ s, $H_t = 4.3$ s, $D = 1.2$ pu
$k_s = 0.6$ pu/elec.rad, $\omega_s = 1$ pu

Appendix B. Operating conditions used for modal analysis in Section 3.1:

$P_{e0} = 0.9$ pu, $_0 = -0.21$, $v_{sd0} = 0$,
$v_{sq0} = 1$ pu $\psi_{sd0} = 1.005$ pu, $\psi_{sq0} = 0$,
$i_{rd0} = 0.345$ pu, $i_{rq0} = 0.7874$,

Appendix C. Controller parameters used for modal analysis in Section 3.1:

$k_{p-idq} = 0.633$ $k_{i-idq} = 8.5$, $k_{p-g} = 0.6$
$k_{i-g} = 2.26$ $k_{p\omega} = 6.98$ $k_{I\omega} = 0.04656$
$k_{p-Q} = 0.01235$ $k_{I-Q} = 4.656$

Appendix D. The participation factors of mode *i* are given by

$$P_i = [p_{1i}p_{2i}\ldots p_{ni}]^T; \quad p_{ki} = \frac{\partial \lambda_i}{\partial a_{kk}} = \psi_{ik}.\phi_{ki}$$

where a_{kj} is the element of jth column and kth row of state matrix A. p_{ki} is a measure of the relative participation of the kth state variable in the ith mode, and vice versa [34].

ψ_{ik} is the kth element of the ith left-eigenvector of state matrix A, and ϕ_{ki} is the kth element of the ith right-eigenvector of state matrix A.

Appendix E. The elements a_{11}, a_{12}, a_{21} and a_{22} of the state matrix in Eq. (38):

$$a_{11} = -\frac{R_s + R_e}{L_s + L_e} - \frac{L_e}{D}\left(i_{gq0} - \frac{L_m}{L_s} i_{rq0}\right) \tag{E.1}$$

$$a_{12} = -\frac{L_s}{L_s + L_e}\left(v_{\infty q0} - \frac{v_{\infty d0} L_e \left(i_{gq0} - \frac{L_m}{L_s} i_{rq0}\right)}{D}\right) \tag{E.2}$$

$$a_{21} = \frac{1 + \frac{L_e}{L_s}}{D} \tag{E.3}$$

$$a_{22} = -\frac{v_{\infty d0}}{D} = \frac{-\frac{R_s + R_e}{L_s}\psi_{sd0} + \frac{R_s + R_e}{L_s} L_m i_{rd0} - R_e i_{gd0}}{D} + \frac{L_e}{D}\left(i_{gq0} - \frac{L_m}{L_s} i_{rq0}\right) \tag{E.4}$$

$$D = \psi_{sd0}\left(1 + \frac{L_e}{L_s}\right) - \frac{L_e L_m}{L_s} i_{rd0} + L_e i_{gd0} \tag{E.5}$$

References

[1] Ackerman T. Wind power in power systems. 2nd ed.. Wiley; 2012.
[2] Pena R, Clare J, Asher G. Doubly fed induction generator using back-to-back PWM converters and its application to variable speed wind energy generation. IEE Proc-Electr Power Appl 1996;143:231–41.
[3] Xu L, Wei C. Torque and reactive power control of a doubly fed induction machine by position sensorless scheme. IEEE Trans Ind Appl 1995;31: 636–642.
[4] Mehta B, Bhatt P, Pandya V. Small signal stability analysis of power systems with DFIG based wind power penetration. Electr Power Energy Syst 2014;58: 64–74.
[5] Tsourakis G, Nomikos BM, Vournas CD. Effect of wind parks with doubly fed asynchronous generators on small signal stability. Electr Power Syst Res 2009;79:190–200.
[6] Dominguez-Garcia JL, Gomis-Bellmunt O, Bianchi FD, Sumper A. Power oscillation damping supported by wind power: a review. Renew Sustain Energy Rev 2012;16:4994–5006.
[7] Mishra Y, Mishra S, Li F. Coordinated tuning of DFIG-based wind turbines and batteries using bacteria foraging technique for maintaining constant grid power output. IEEE Trans Power Syst 2012;6(1):16–26.
[8] Mishra Y, Mishra S, Tripathy M, Senroy N, Dong ZY. Improving stability of a DFIG-based wind power system with tuned damping controller. IEEE Trans Energy Convers 2009;24(3):650–60.
[9] Hughes FM, Anaya-Lara O, Jenkins N, Strbac G. Control of DFIG-based wind generation for power network support. IEEE Trans Power Syst 2005;20 (4):1958–66.
[10] Nunes MVA, Lopes JAP, Zurn HH, Bezerra UH, Almeuda RG. Influence of variable-speed wind generators in transient stability margin of the conventional generators integrated in electrical grids. IEEE Trans Energy Convers 2004;19:692–701.
[11] Pannell G, Atkinson DJ, Zahawi B. Analytical study of grid-fault response of wind turbine doubly fed induction generator. IEEE Transactions on Energy Conversion 2010;25:1081–91.
[12] Rola x, n A Co, rcoles F, Pedra J. Doubly fed induction generator subject to symmetrical voltage sags. IEEE Transactions on Energy Conversion 2011;26:1219–29.
[13] Lopez J, Sanchis P, Roboam X, Marroyo L. Dynamic behavior of the doubly fed induction generator during three-phase voltage dips. IEEE Trans Energy Convers 2007;22:709–17.
[14] Morren J, de Haan SW. Short-circuit current of wind turbines with doubly fed induction generator. IEEE Trans Energy Convers 2007;22:174–80.
[15] Lopez J, Sanchis P, Roboam X, Marroyo L. Wind turbines based on doubly fed induction generator under asymmetrical voltage dips. IEEE Trans Energy Convers 2008;23:331 (330).
[16] El-Sattar AA, Saad NH, Shams El-Dein MZ. Dynamic response of doubly fed induction generator variable speed wind turbine under fault. Electr Power Syst Res 2008;78:1240–6.
[17] Rahimi M, Parniani M. Grid-fault ride-through analysis and control of wind turbines with doubly fed induction generators. Electr Power Syst Res 2010;80:184–95.
[18] Rahimi M, Parniani M. Coordinated control approaches for low-voltage ride-through enhancement in wind turbines with doubly fed induction generators. IEEE Trans Energy Convers 2010;25:873–83.
[19] Rahimi M, Parniani M. Efficient control scheme of wind turbines with doubly-fed induction generators for low voltage ride-through capability enhancement. IET J Renew Power Gener 2010;4:242–52.
[20] Rahimi M, Parniani M. Low voltage ride-through capability improvement of DFIG-based wind turbines under unbalanced voltage dips. Electr Power Energy Syst 2014;60:82–95.
[21] Anaya-Lara O, Hughes FM, Jenkins N, Strbac G. Contribution of DFIG- based wind farms to power system short-term frequency regulation. IEE proceedings on generation, transmission and distribution 2006;153:164–70.
[22] Ramtharan G, Ekanayake JB, Jenkins N. Frequency support from doubly fed induction generator wind turbines. IET J Renew Power Gener 2007;1:3–9.
[23] Mauricio JM, Marano A, Gomez-Exposito A, MartinezRamos JL. Frequency regulation contribution through variable-speed wind energy conversion systems. IEEE Trans Power Syst 2009;24:173–80.
[24] Holdsworth L, Wu XG, Ekanayake JB, Jenkins N. Comparison of fixed speed and doubly-fed induction wind turbines during power system disturbances. IEE proceedings on generation, transmission and distribution 2003;150:343–52.
[25] Sun T, Chen Z, Blaabjerg F. Transient stability of DFIG wind turbines at an external short-circuit fault. Wind Energy 2005;8:345–60.
[26] Muyeen S, Ali M, Takahashi R, Murata T, Tamura J. Damping of blade-shaft torsional oscillations of wind turbine generator. Electr Power Compon Syst 2008;36:195–211.
[27] Lin L, Song L, Li W, Jing S. Modal analysis concerning the control mode of doubly-fed induction generator. In: Proceedings of the international conference on sustainable power generation and supply; 2009, p. 1–6.
[28] Yang L, Xu Z, ostergaard J, Dong Z, Wong K, Ma X. Oscillatory stability and eigenvalue sensitivity analysis of a DFIG wind turbine system. IEEE Trans Energy Convers 2011;26:328–39.
[29] Wu F, Zhang XP, Godfrey K, Ju P. Small signal stability analysis and optimal control of a wind turbine with doubly fed induction generator. IEE proceedings on generation, transmission and distribution 2007;1:751–60.

[30] Wu F, Zhang XP, Godfrey K, Ju P. Modeling and control of wind turbine with doubly fed induction generator. Proceedings of IEEE PSCE 2006:1404–9.
[31] Mei F, Pal BC. Modal analysis of grid-connected doubly fed induction generators. IEEE Trans Energy Convers 2007;22:728–36.
[32] Mei F, Pal BC. Modeling and small-signal analysis of a grid connected doubly-fed induction generator. In: Proceedings of IEEE general meeting of power system society; 2005, p. 2101–8.
[33] Rouco L, Zamora JL. Dynamic patterns and model order reduction in small-signal models of doubly fed induction generators for wind power applications. In: Proceedings of IEEE general meeting of power system society; 2006.
[34] Kundur P. Power system dynamics and control. 2nd ed.. New York: McGraw Hill; 1994.